Research Article | Vol. 27, No. 17 / 19 August 2019 / Optics Express 24670

Optics EXPRESS

Output energy enhancement in a mode-locked Er-doped fiber laser using CVD-Bi_2Se_3 as a saturable absorber

QUANXIN GUO,[1] JIE PAN,[1] YANJUN LIU,[2] HAIPENG SI,[3] ZHENGYI LU,[1] XILE HAN,[1] JINJUAN GAO,[1] ZITAN ZUO,[1] HUANIAN ZHANG,[1,4] AND SHOUZHEN JIANG[1,5]

[1] *Collaborative Innovation Center of Light Manipulations and Applications in Universities of Shandong, Shandong Normal University, Jinan 250014, China*
[2] *Department of Electrical and Electronic Engineering, Southern University of Science and Technology, Shenzhen 518055, China*
[3] *Department of Orthopaedics, Qilu Hospital, Shandong University, Jinan 250012, China*
[4] *huanian_zhang@163.com*
[5] *jiang_sz@126.com*

Abstract: In this study, the output energy in topological insulators (TIs)-based Erbium-doped fiber laser (EDFL) was improved using two strategies: bidirectional pumped laser cavity and saturable absorber (SA) with high damage threshold and large modulation depth. Using the chemical vapor deposition (CVD) method, Bismuth Selenide (Bi_2Se_3) film was synthesized and improved to a SA. Employing this CVD-Bi_2Se_3 SA in an EDFL, bright and bright-dark soliton operations were achieved. The average output power/pulse energy was 82.6 mW/48.3 nJ and 81.2 mW/47.5 nJ, respectively. The results demonstrate that CVD-Bi_2Se_3 can act as an excellent performance material to improve output power performance in TISA-based EDFL.

1. Introduction

Mode-locked fiber lasers are desired by variety of applications, e.g. optical communications, optical sensing, material processing, biomedical diagnostics and spectroscopy [1–3]. A main strategy was typically used to obtain mode-locked operations in fiber lasers: incorporating a saturable absorbers (SAs) whose optical transmittance increases with the increase in the light intensity in a laser cavity. Recently, graphene [4–8] and other two-dimensional (2D) materials (e.g. topological insulators (TIs) [9–21], transition metal dichalcogenides (TMDs) [22–30], black phosphorus (BP) [31–34] and so on [35–38]) is preferred for SA production due to its strong optical nonlinearity, broad spectral absorption, ultrafast response time and the ease of all-fiber integration [39]. Because of the ever-growing demand for mode-locked fiber lasers, high-performance SAs made of 2D materials have aroused rising attention.

Recently, a class of materials called TIs, e.g. Bismuth Selenide (Bi_2Se_3), Bismuth Telluride (Bi_2Te_3) and Antimony Telluride (Sb_2Te_3), have been demonstrated to be excellent 2D materials to fabricate SAs for Yb, Er and Tm-doped mode-locked fiber lasers [9–21]. Among them, Bi_2Se_3 is prominent for its properties of low saturation intensity, ultrafast recovery time, large modulation depth and high damage threshold. Besides, Bi_2Se_3 as a type of Dirac material, has a topologically non-trivial bandgap of 0.3 eV, corresponding to a wide optical absorption range, offering the possibility to be used as a SA when the wavelength of the light is shorter than 4 μm. Moreover, due to the giant third order nonlinearity of Bi_2Se_3, various mode-locked operations could be achieved in Bi_2Se_3 SA based fiber lasers. In 2012, Zhao *et al.* reported a wavelength-tunable picosecond mode-locked fiber laser with Bi_2Se_3 SA [9]. Since then, diverse Bi_2Se_3 SA based mode-locked fiber lasers have been demonstrated in a couple of years. Previous contributions

#364494 https://doi.org/10.1364/OE.27.024670
Journal © 2019 Received 8 Apr 2019; revised 20 Jun 2019; accepted 6 Aug 2019; published 15 Aug 2019

Optics EXPRESS

were mainly focus on the operation in conventional soliton state. However, the output power of TISA based mode-locked fiber lasers still needs to be further improved. To the best of our knowledge, the average output power of TISA based mode-locked fiber lasers is generally lower than 10 mW. Yan *et al.* experimentally demonstrated a mode-locked Er-doped fiber laser (EDFL) with Bi_2Te_3 SA, of which the maximum average output power of the harmonic soliton pulse is 45.3 mW with a reputation rate of 2.95 GHz, corresponding a single pulse energy of 15.4 pJ [40]. Besides, for Bi_2Se_3 SA based mode-locked fiber lasers, the reported maximum average output power is even lower. In 2018, Xu *et al.* demonstrated a Bi_2Se_3 SA based mode-locked EDFL, which could achieve various mode-locked pulses generations, including large-energy pulses, dark solitons and soliton rains [41]. At the soliton rains mode-locked state, the maximum average output power is 33.8 mW, which is the largest value of output power in ever reported Bi_2Se_3 SA based mode-locked fiber laser. Those limitations could be overcome by employing high-quality Bi_2Se_3 SAs with a high optical damage threshold that could operate at high-power condition are essential. Up to date, mode lockers based on Bi_2Se_3 were prepared by polyol method and liquid-phase exfoliation (LPE) method. These methods are capable of controlling the phase formation, particle size and morphology of the Bi_2Se_3 nanosheets and have the advantages of easy-preparation, low cost, etc. However, with the above method, the crystalline quality of the obtained Bi_2Se_3 nanosheets is not sufficiently excellent, and the particle size is in a small scale. To solve this problem, a suitable synthesis method should be introduced to prepare Bi_2Se_3 SA. As we know, chemical vapor deposition (CVD) is an effective method for synthesizing high-crystalline quality layered 2D materials. Furthermore, the layer numbers of 2D materials fabricated via CVD method are controllable and the shapes are uniform. In general, using CVD method, the saturation intensity and modulation depth are controllable via changing the layer number, and the damage threshold could be much higher than any other synthesis method due to the excellent crystalline quality.

In this paper we demonstrated an EDFL mode-locked by a CVD- Bi_2Se_3 SA, which achieved two different mode-locked operations. The CVD-Bi_2Se_3 SA can serve as an excellent device to achieve diverse high pulse operations in fiber lasers for its properties of excellent saturable absorption, highly nonlinear effect and high damage threshold. For the bright and bright-dark soliton operations, the maximum average output power/single pulse energy was 82.6 mW/48.3 nJ and 81.2 mW/47.5 nJ with a pump power of 1.7 W, respectively. To the best of our knowledge, in constant to the reported TISA based mode-locked EDFL, 82.6 mW is the highest average output power. As a result, using CVD-Bi_2Se_3 SA and pumped by two pump sources, the output power is improved in TISA based EDFL.

2. CVD- Bi_2Se_3 SA fabrication and characterization

The Bi_2Se_3 sheets synthesizing experiment was carried out in the horizontal tube furnace (OTL1200) using a two-step growing process. See the details of the progress in Fig. 1. First, deposit a Se layer on the SiO_2 substrate as a seed layer to produce nucleation sites around Se and force the Bi_2Se_3 sheets growing with a lateral direction. Besides, the Se-rich environment, provided by the seed layer, was necessary to increase the Se: Bi flux ratio. Se powder is used as the evaporation source in the center of the constant temperature zone. In the meantime, a SiO_2 substrate cleaned using ultrasonic machine with the solutions of acetone, ethyl alcohol and deionized water was placed in the downstream zone, 15 cm far away from the Se powder. At a ramping rate of 10 ℃/min and the Ar gas flow of 50 sccm, the Se layer was deposited on the SiO_2 substrate at the target temperature of 200 ℃ for 20 min under a base pressure of 2 Pa. Second, the Bi_2Se_3 sheets started to grow on the Se/SiO_2 substrate using CVD method. Bi_2Se_3 powder, as the source material, was positioned near the hot center region where the temperature is close to the preset temperature (550 ℃). The Se/SiO_2 substrate was placed in the downstream zone (15 cm far from the Bi_2Se_3 powder). The quartz tube was purged with Ar gas, and then the

Optics EXPRESS

source material was deposited on the substrate, carried by the Ar with a gas flow of 50 sccm. To avoid the Se from the Se/SiO_2 substrate being volatilized and to ensure the Bi_2Se_3 sheets can be deposited uniformly, the part of the tube containing the source material and substrate was removed from the furnace during the ramping process. It took about 55 min to rise the temperature to 550 ℃ at a ramping rate of 10 ℃/min. The part of the quartz tube containing the source material and substrate was moved to the center of the furnace, while the furnace was heated to the preset temperature of 550 ℃. The Bi_2Se_3 sheets started to grow for 20 min when the temperature was stabilized. Finally, the quartz tube was naturally cooled down to the ambient temperature in an Ar atmosphere.

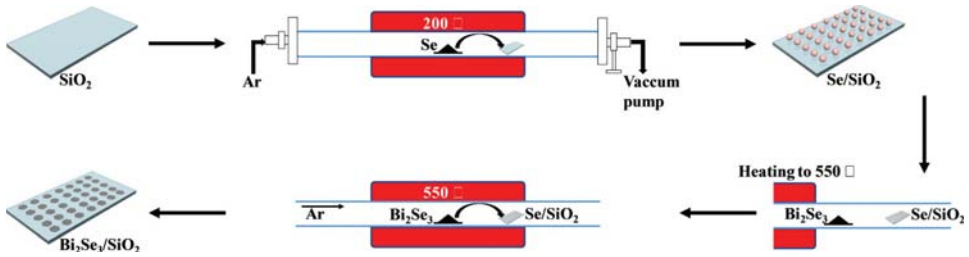

Fig. 1. Schematic of the experimental setup for the synthesis of Bi_2Se_3 sheets.

To incorporate the synthesized Bi_2Se_3 sheets into a fiber laser, the thermal release tape was used to transfer the CVD- Bi_2Se_3 from the SiO_2 substrate onto a fiber ferrule. The transfer process is illustrated in Fig. 2. First, the thermal release tape was mounted upside down, facing the Bi_2Se_3/SiO_2, and pressed with a finger (or something else) to be bonded to the material. Subsequently, the tape with a few layers Bi_2Se_3 sheets was stripped off from the substrate and stick on a fiber head. A heating platform was used to release the material from the thermal release tape. When the platform was raising to 120 ℃, the fiber ferrule/tape was moved onto the platform and kept for ~ 5 min till the tape was separated from the fiber head. Finally, few layers Bi_2Se_3 sheets was transferred to the fiber head and SA was successfully prepared.

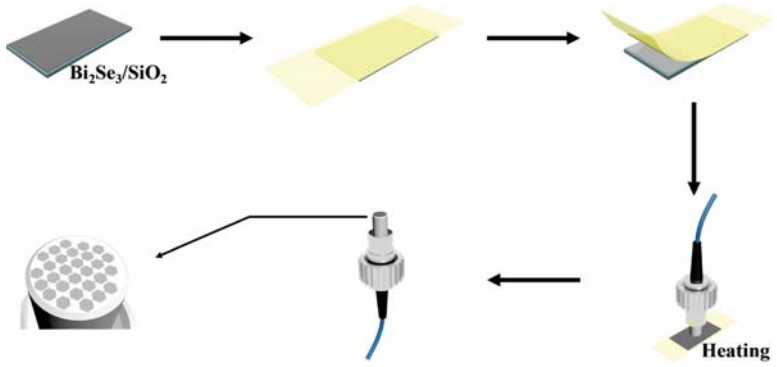

Fig. 2. Preparation process of the CVD-Bi_2Se_3 SA.

The surface morphologies of the sample were imaged under a scanning electron microscope (SEM, ZEISS Sigma 500). The SEM image in Fig. 3(a) shows the hexagonal morphology of the uniform Bi_2Se_3 nanosheet with a multi-layered structure. The size of the nanosheet was measured to be a few microns. The synthesized sample was further measured under an atomic force microscope (AFM, Bruker Multimode 8) to characterize the thickness of Bi_2Se_3

Optics EXPRESS

nanosheet. As shown in Fig. 3(b), the AFM image clearly exhibits the surface morphology of the Bi_2Se_3 nanosheet with a layered-hexagonal structure. Figure 3(c) shows the difference in height from the substrate to the Bi_2Se_3 nanosheet, which corresponds to the thickness of about 120 nm of the synthesized sample. To characterize the Bi_2Se_3 incorporated in the fiber laser, the synthesized Bi_2Se_3 was transferred onto a SiO_2 substrate using a thermal release tape, and the corresponding SEM and AFM image were measured respectively. Figure 3(d) shows the SEM image with a resolution of 20 μm. The irregular nanosheets were randomly distributed on the substrate, suggesting the transfer method was extremely effectual. The transferred nanosheets were micron-sized, offering the possibility to ensure that the Bi_2Se_3 can cover the fiber core after the preparation process of SA. The AFM image was recorded to analyze the thickness of the transferred nanosheets, as shown in Fig. 3(e), and the corresponding height difference from the substrate to the Bi_2Se_3 nanosheet is shown in Fig. 3(f). The thickness of the transferred sheet was 27 nm, much lower than that of the synthesized sample, which allows for a good optical transmittance.

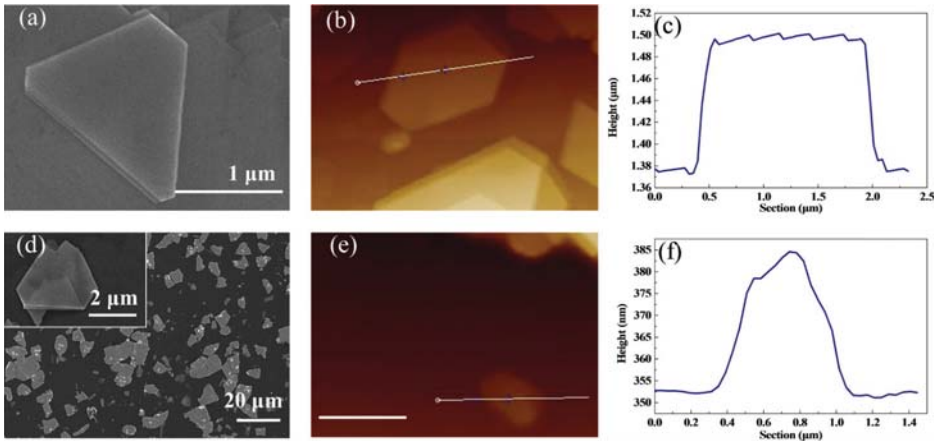

Fig. 3. (a) SEM image of the CVD-Bi_2Se_3, (b) AFM image of the Bi_2Se_3, and (c) height profile of the selected area in (b); characteristics of the transferred Bi_2Se_3 sheet: (d) SEM image, (e) AFM image, and (f) height profile of the selected area in (e).

The chemical composition of the synthesized sample was measured under the energy dispersion spectroscopy (EDS) in the SEM system. As shown in Fig. 4(a), the EDS spectrum demonstrated the recorded signals of C, O, Si, Se, and Bi. The signal of C atomic was attributed to the Carbon tape that used to hold the measured sample. The peaks of Si and O are assigned to the SiO_2 substrate. The ratios of C, O, Si, Se, and Bi are 29.17, 2.98, 9.84, 34.63 and 23.39, respectively, as shown in the inset of Fig. 4(a). The atomic ratio of Se and Bi is 1.48: 1, which reveals a high purity of the synthesized Bi_2Se_3. It is noteworthy that the atomic ratio of O and Si is 0.30: 1, which is not consistent with the actual ratio in the SiO_2 substrate. This phenomenon might due to the inherent nature of the EDS instrument. It is generally known that since the detection voltage is difficult to be completely suitable, the atomic ratios of the elements with a small atomic number (e.g. Carbon, Nitrogen and Oxygen) measured using EDS technology are unreliable. Therefore, the measured atomic ratio of O atomic does not have much reference value.

Structural characterization of the synthesized Bi_2Se_3 sheets was tested using a Raman spectroscopy (Horiba HR Evolution 800). In the range of 50-200 cm^{-1}, the Raman spectrum was recorded with a 532 nm laser for excitation at ambient temperature, as shown in Fig. 4(b). The figure reveals that there are three characteristic peaks appeared in the Raman spectrum: the out-of-plane vibrational mode A_{1g}^1 at 71.3 cm^{-1}, in-plane vibrational mode E_g^2 at 129.8 and

Optics EXPRESS

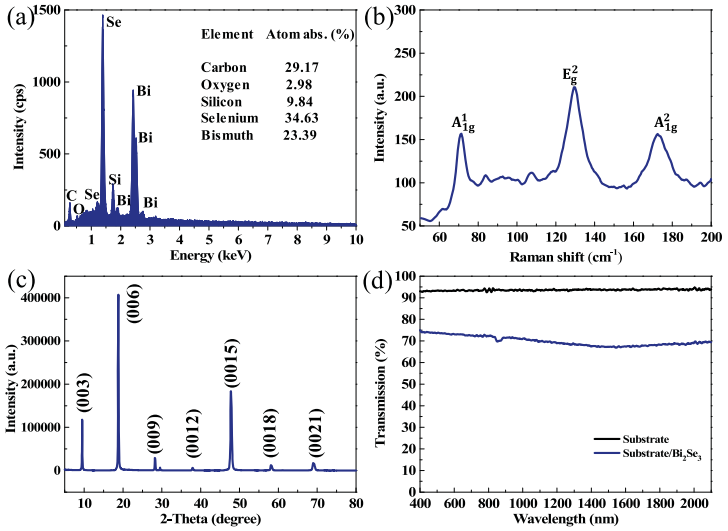

Fig. 4. Characteristics of the Bi_2Se_3 sheet: (a) EDS spectrum, (b) typical Raman spectrum, (c) XRD pattern, and (d) linear transmission of the transferred Bi_2Se_3 sheet.

the out-of-plane vibrational mode A_{1g}^2 at 172.0 cm^{-1}. This result confirmed that the Bi_2Se_3 crystal was synthesized. X-ray diffraction (XRD, Bruker D8) was performed to explore the phase structure of the Bi_2Se_3 sample, as shown in Fig. 4(c). The (003) family diffraction peaks, which includes (003), (006), (009), (0012), (0015), (0018), and (0021) were detected, suggesting that the synthesized Bi_2Se_3 was rhombohedral structure along C axis [0001]. All the diffraction peaks exhibit high intensity, which evidences the high crystalline quality of our Bi_2Se_3 sheet grown by CVD method.

To characterize the absorption property of the synthesized Bi_2Se_3, the linear transmittance spectra of the Bi_2Se_3/SiO_2 (after a transfer process) and SiO_2 substrate were investigated using a UV/Vis/NIR spectrophotometer, as shown in Fig. 4(d). In comparation to the SiO_2 substrate, the maximum transmittance of Bi_2Se_3/SiO_2 in the wavelength range of 400-2100 nm was decreased from 94% to 69%. The minimum transmittance was 66.86% while the corresponding light wavelength was 1544 nm, which was close to the operating wavelength of our EDFL. Obviously,

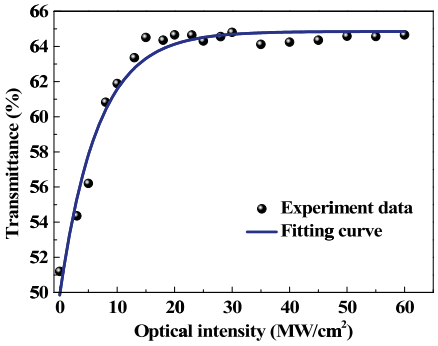

Fig. 5. The nonlinear absorption curve of the Bi_2Se_3 SA.

Optics EXPRESS

the Bi_2Se_3 sheets had a wide optical absorption range due to the bandgap of 0.3 eV. This feature allows Bi_2Se_3 to work as SAs when the wavelength of the light is shorter than 4 μm.

Using the power-dependent transmission technique and a homemade nonlinear polarization rotation (NPR) EDFL with a pulse width of 560 fs at 1560.3 nm and a repetition rate of 33.6 MHz, the nonlinear saturable absorption property of the prepared Bi_2Se_3 SA was investigated. In the experiment, the Bi_2Se_3 SA exhibited an excellent saturable absorption property. As shown in Fig. 5, the fitting curve shows that the saturation intensity and modulation depth are 6.59 MW/cm^2 and 15%, respectively.

3. Experimental setup

The experimental setup is schematically shown in Fig. 6. A 974 nm laser diode (LD) and a 976 nm LD with the maximum output power of 544 mW and 1294 mW was used to provide bidirectional pump, and two 980/1550 wavelength-division multiplexers (WDM) were used to deliver the pump energy into the cavity. A piece of 62 cm long Er-doped fiber (EDF, Liekki Er-80, 8/125) with a dispersion parameter of 15.7 ps/nm/km served as the gain medium. The peak core absorption and $Er^{3\pm}$ concentration were 80 dB/m and 3150 ppm, respectively. There were two PCs to adjust the cavity birefringence in our fiber laser. Besides, a polarization-independent isolator (PI-ISO) was used to force the unidirectional operation of the ring cavity. The 60/40 optical coupler (OC) was used to extract the output of the laser pulses. To regulate the net dispersion value of the cavity, a 100 m long single-mode fiber (SMF, SMF-28) with dispersion parameter of 17 ps/nm/km was added into the cavity. The total length and net cavity dispersion were 120.2 m and -2.603 ps^2, respectively.

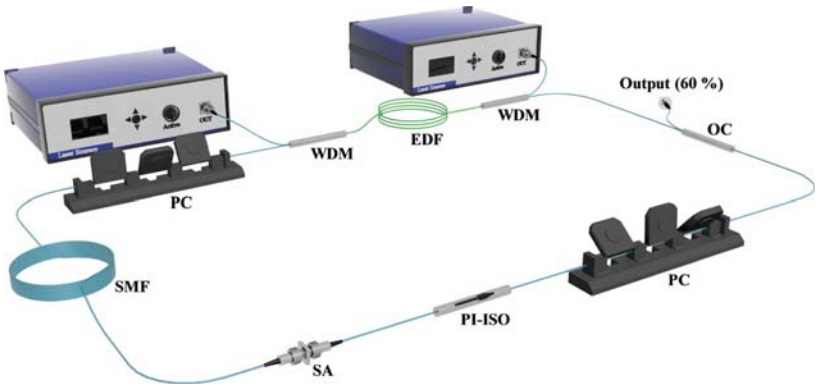

Fig. 6. The experimental setup of the passively mode-locked fiber laser.

4. Results and discussion

It is generally known that self-mode-locked operation can be achieved sometimes with a long-length laser cavity. Hence, before carrying out this experiment, we tested the operation characteristic of the EDFL without the Bi_2Se_3 SA. No pulse generation had been observed by carefully adjusting the PCs and the pump power, which implies that the self-mode-locked or the Fabry-Perot cavity effect does not exist in this laser cavity. After the Bi_2Se_3 SA was inserted into the ring laser cavity, different stable mode-locked operations could be achieved by adjusting the pump power and the state of polarization controlled by the PCs. In the following, two mode-locked operations that had been achieved in our EDFL are to be reported.

In this section, we primarily discussed the bright-soliton mode-locked state performance at the pump power of 1.7 W in our EDFL, as shown in Fig. 7. Figure 7(a) shows the typical output

Optics EXPRESS

optical spectrum with the center wavelength located at 1557.908 nm. The corresponding 3-dB bandwidth was 0.342 nm. The single pulse trace shown in Fig. 7(b) has a pulse width of about 7.78 ns. This wide pulse duration was primarily attributed to the large net dispersion value, which was caused by the long-length laser cavity. The typical pulse train shown in the inset of Fig. 7(b) reveals that the pulse-to-pulse interval was 0.58 μs, which was well consistent with the 1.71 MHz fundamental frequency and the 120.2 m cavity length as well. This suggests that the pulse laser operated at the mode-locked state. To test the stability of this mode-locked operation, the RF spectrum was recorded, as shown in Fig. 7(c). The fundamental frequency was located at 1.71 MHz with a signal to noise ratio (SNR) of 42 dB. It noteworthy that the signal measured by the spectrum analyzer was only 25% of the output power. Consequently, the actual SNR should be higher than 42 dB. The achieved pulse duration was on a ns level, and the shape of the pulse did not exhibit a Gaussian or Hyperbolic secant profile. Thus, the RF spectrum tested in a broader range was not obtained in our experiment. The relations between the average output power and the pump power is shown in Fig. 7(d). The laser started to operate at the mode-locked state when the pump power was 600 mW. Obviously, the output power risen from 48.3 to 82.6 mW with the increase in the pump power from 0.6 to 1.7 W, and the corresponding single pulse energy rose from 26.8 nJ to 48.3 nJ. To the best of our knowledge, 82.6 mW is the largest value of the average output power in TISA based mode-locked EDFL.

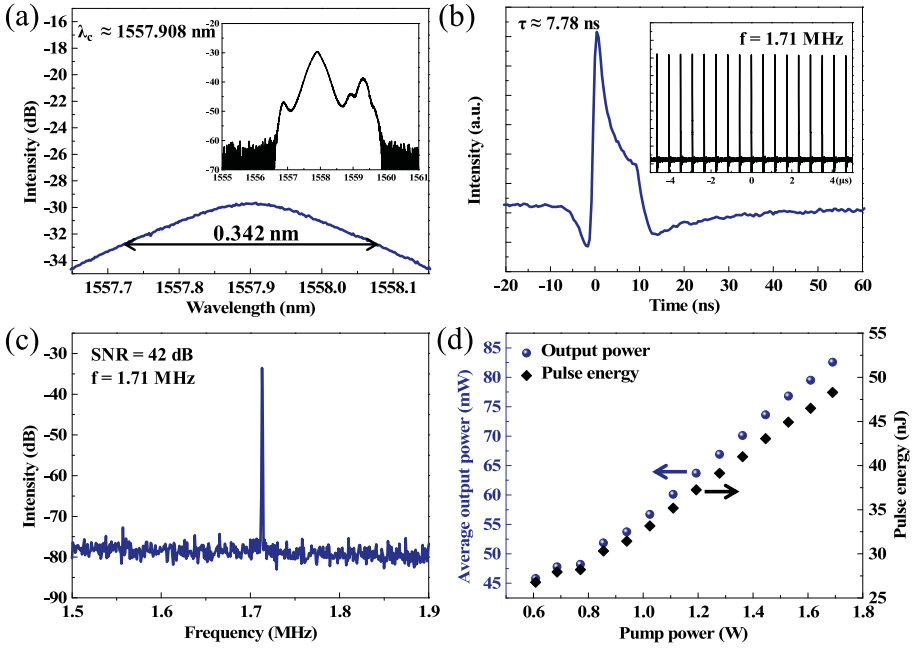

Fig. 7. Characteristics of the dual-wavelength bright-soliton pulse laser: (a) output optical spectrum, (b) single pulse trace and the inset is digital oscilloscope image, (c) RF spectrum, and (d) the relationship between the average output power, single pulse energy, and the pump power.

Due to the giant third-order nonlinear optical (NLO) coefficient, Bi_2Se_3 SA exhibits excellent NLO effect, which makes it likely to achieve versatile mode-locked operations, e.g. multi-wavelength pulse, rectangular pulse and multi-soliton generation. In our experiment, after the polarization state of the laser cavity was regulated by carefully adjusting the two PCs, another stable mode-locked state, the bright-dark soliton pair operation, was achieved in our Bi_2Se_3 based EDFL at the pump power of 551 mW. It is worth noting that the mode-locked threshold of both

Optics EXPRESS

two mode-locked operations are relatively high. This phenomenon was mainly caused by the large insertion loss of the Bi_2Se_3 SA. After testing, the insertion loss of the SA is 6.6 dB, which is enough to cause an increase in the threshold. In addition, the value of the modulation depth of the Bi_2Se_3 SA was 15%, together with the large insertion loss, leads to a high mode-locked threshold. The characteristics of the bright-dark soliton pair mode-locked pulse laser are shown in Fig. 8. The typical triple-wavelength optical spectrum in Fig. 8(a) obviously shows that the center wavelengths of the two separated spectra were 1556.876, 1558.332 and 1559.386 nm with 3-dB bandwidth of 0.209, 0.354 and 0.235 nm, respectively. As mentioned above, Bi_2Se_3 has extremely high NLO coefficient that the NLO effect in the Bi_2Se_3 based mode-locked EDFL is overly strong. In particular, the Bi_2Se_3 synthesized using CVD method has a large area in a μm-scale, so its NLO effect should be higher. Besides, the polarization of the PCs could combine with the birefringence effect of the SMF to generate the spectral filtering effect, thereby achieving the multi-wavelength pulse. The trace of a single pulse, containing both bright and dark soliton simultaneously, is shown in Fig. 8(b). In accordance with the soliton theory and the previously work of Guo *et al.* in 2015, this pulse profile was termed as bright-dark soliton pair that exhibits the shape-preserving property of soliton [17]. The analysis of the trace shown in Fig. 8(b) reveals that the pulse durations of the bright and dark pulse were 2.59 and 5.59 ns, respectively. The difference with symbiotic solitary-wave pairs is that our bright and dark soliton are different in the pulse width, which is attributed to the high NLO effect caused by the Bi_2Se_3 SA. The pulse train recorded with a bandwidth of 10 μs is shown in the inset of Fig. 8(b). The figure shows that the pulse-to-pulse interval was 0.58 μs, which corresponded to the total length of the laser cavity of 120.2 m. The RF spectrum was recorded to demonstrate the stability of the EDFL, as shown in Fig. 8(c). The SNR is 41 dB with the fundamental frequency of 1.71 MHz. For the same mentioned reason, the actual value of SNR should be larger than the recorded value. Figure 8(d) displayed the output energy performance of the EDFL. With the rise in the pump power from 0.55 W to 1.7 W, the average output power increased from 40.1 to 81.2 mW, and the pulse energy rose from 23.5 to 47.5 nJ.

It is worth mentioning that the saturation absorption was not due to the direct-bandgap absorption, because the laser was operated at 1.5 μm region and the corresponding photon energies were about 0.83 eV, larger than the topologically non-trivial bandgap of Bi_2Se_3 (0.3 eV). Due to the Dirac-like band structure of Bi_2Se_3 and Pauli blocking, the saturation absorption effect will occur by the excitation from a strong light with single-photon energy larger than the bandgap [42].

Several representative EDFLs based on TISA were summarized in Table 1 to highlight the output energy performance of our CVD-Bi_2Se_3 based EDFL. The mode-locked pulse with the output power of 45.3 mW was achieved in a Bi_2Te_3 mode-locked EDFL [40]. However, the pulse energy was limited to 15.36 pJ. The Bi_2Se_3 EDFL listed in the table achieved the soliton rain mode-locked state with an output power of 33.8 mW [41]. However, the single pulse rain contains several soliton pulses so that the single pulse energy should be lower than the pulse energy of 62.87 nJ. In our study, the values of average output power and pulse energy were up-regulated significantly. 82.6 mW is not only the peak of the average output power compared with the mentioned TISA based EDFL, but also an extra high value compared with the other SAs-based EDFL. Differently with the mentioned works, a large pulse energy was obtained simultaneously in our experiment. Since CVD-Bi_2Se_3 exhibits high-crystalline quality, the damage threshold of the Bi_2Se_3 SA was extremely large, offering the ability to support the high pulse energy. Additionally, the CVD-Bi_2Se_3 has a low saturable intensity of 6.59 MW/cm^2 and a large modulation depth of 15%, offering the possibility to generate the ultrafast and high-energy pulse. This suggests that Bi_2Se_3 grown by CVD method can exhibit a high performance in the laser applications.

Optics EXPRESS

Table 1. A Comparison of Passively Mode-locked EDFL Based on TISA[α]

SA material	Platform	α_s (%)/I_{sat} (MW · cm^{-2})	Wavelength (nm)	Output power (mW)	Pulse energy (nJ)	Ref.
Bi_2Se_3 (LPE)	Fiber ferrule	5.2/12	1560	0.86	0.023	12
Bi_2Se_3 (LPE)	Fiber ferrule	3.8/25	1567-1569	9.7	1.1	43
Bi_2Se_3 (LPE)	Fiber ferrule	4.1/26	1561.6/1562.1	10	2.82	16
Bi_2Se_3 (LPE)	Fiber ferrule	3.9/12	1557.5	1.8	0.14	11
Bi_2Se_3 (LPE)	Fiber ferrule	6.9/7.06	1560.5	33.8	62.87	41
Bi_2Te_3 (LPE)	Fiber ferrule	2/180	1557	0.4	0.046	44
Bi_2Te_3 (ME)	Side-polished fiber	15.7/—	1547	0.8	0.053	45
Bi_2Te_3 (LPE)	Fiber ferrule		1558.12	0.59	0.485	46
			~ 1558	0.73	0.6	
			~ 1558	0.82	0.674	
Bi_2Te_3	Fiber ferrule	10.39/6.48	1571	11	1.03	47
			—	~ 30	2.801	
Bi_2Te_3 (PLD)	Microfiber	6.2/28	1564	45.3	15.36 pJ	40
Sb_2Te_3 (ME)	Side-polished fiber	6/31	1565	1	44.8 pJ	48
Sb_2Te_3 (PVD)	Side-polished fiber	14.9/228	1564.6	6.2	0.19	49
			1564.6	4.2	0.13	
			1568.8	9	0.27	
Sb_2Te_3 (ME)	Side-polished fiber	6/31	1561	1	29 pJ	50
Sb_2Te_3 (LPE)	Side-polished fiber	3.9/106	1556	0.9	39.6 pJ	51
Sb_2Te_3 (ME)	Fiber ferrule	—/—	1558.6	0.5	0.105	52
Sb_2Te_3 (ME)	Fiber ferrule	—/—	1558.5	0.5	0.133	18
			1558.2	4.5	14.8 pJ	
Sb_2Te_3	Fiber ferrule	13/212.3	1558	5.34	0.21	53
Sb_2Te_3 (PLD)	Microfiber	7.42/175	1530	12	0.127	54
Bi_2Se_3 (CVD)	Fiber ferrule	15/6.59	1557.908	82.6	48.3	Our work
			1556.876/ 1558.332/ 1559.386	81.2	47.5	

[α] α_s, modulation depth; I_{sat}, saturable intensity; ME, mechanical exfoliation; PVD, pulsed magnetron sputtering.

Optics EXPRESS

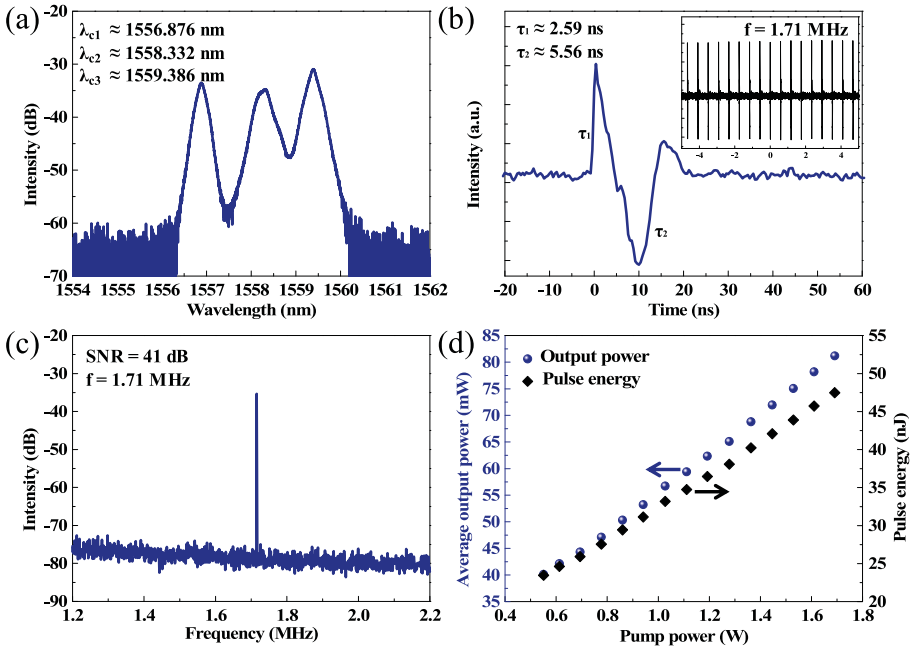

Fig. 8. Characteristics of the triple-wavelength bright-dark soliton pair: (a) output optical spectrum, (b) single pulse trace and the inset is digital oscilloscope image, (c) RF spectrum, and (d) the relationship between the average output power, single pulse energy, and the pump power.

5. Conclusion

To sum up, the output energy performance of TISA based EDFL was enhanced using bidirectional pumped laser cavity and the CVD grown Bi_2Se_3 SA which has a large damage threshold. Using this CVD-Bi_2Se_3 SA in an EDFL, the 82.6 mW/48.3 nJ bright mode-locked pulse and 81.2 mW/47.5 nJ bright-dark soliton pair pulse were achieved easily. To the best of our knowledge, 82.6 mW is the largest value of the average output power in TISA based mode-locked EDFL. According to the results, the CVD-Bi_2Se_3 with the large modulation depth, third order nonlinearity and damage threshold could act as an excellent SA material to improve the output energy performance in mode-locked fiber lasers.

Funding

National Natural Science Foundation of China (11674199, 51707111, 61205174); Natural Science Foundation of Shandong Province (2017GGX20120, ZR2016FP01, ZR2018QF006); China Postdoctoral Science Foundation (2016M602177).

References

1. L. E. Nelson, D. J. Jones, K. Tamura, H. A. Haus, and E. P. Ippen, "Ultrashort-pulse fiber ring lasers," Appl. Phys. B: Lasers Opt. **65**(2), 277–294 (1997).
2. U. Keller, "Recent developments in compact ultrafast lasers," Nature **424**(6950), 831–838 (2003).
3. M. E. Fermann and I. Hartl, "Ultrafast fibre lasers," Nat. Photonics **7**(11), 868–874 (2013).
4. H. Zhang, D. Y. Tang, R. J. Knize, L. M. Zhao, Q. L. Bao, and K. P. Loh, "Graphene mode locked, wavelength-tunable, dissipative soliton fiber laser," Appl. Phys. Lett. **96**(11), 111112 (2010).
5. D. Popa, Z. Sun, F. Torrisi, T. Hasan, F. Wang, and A. C. Ferrari, "Sub 200 fs pulse generation from a graphene mode-locked fiber laser," Appl. Phys. Lett. **97**(20), 203106 (2010).

Optics EXPRESS

6. Z. Sun, T. Hasan, F. Torrisi, D. Popa, G. Privitera, F. Wang, F. Bonaccorso, D. M. Basko, and A. C. Ferrari, "Graphene mode-locked ultrafast laser," ACS Nano **4**(2), 803–810 (2010).
7. Z. T. Wang, Y. Chen, C. J. Zhao, H. Zhang, and S. C. Wen, "Switchable dual-wavelength synchronously Q-switched erbium-doped fiber laser based on graphene saturable absorber," IEEE Photonics J. **4**(3), 869–876 (2012).
8. F. Bonaccorso, Z. Sun, T. Hasan, and A. C. Ferrari, "Graphene photonics and optoelectronics," Nat. Photonics **4**(9), 611–622 (2010).
9. C. J. Zhao, Y. H. Zou, Y. Chen, Z. T. Wang, S. B. Lu, H. Zhang, S. C. Wen, and D. Y. Tang, "Wavelength-tunable picosecond soliton fiber laser with topological insulator: Bi_2Se_3 as a mode locker," Opt. Express **20**(25), 27888–27895 (2012).
10. Y. C. Meng, G. Semaan, M. Salhi, A. Niang, K. Guesmi, Z. C. Luo, and F. Sanchez, "High power L-band mode-locked fiber laser based on topological insulator saturable absorber," Opt. Express **23**(18), 23053–23058 (2015).
11. H. Liu, X. W. Zheng, M. Liu, N. Zhao, A. P. Luo, Z. C. Luo, C. J. Zhao, and S. C. Wen, "Femtosecond pulse generation from a topological insulator mode-locked fiber laser," Opt. Express **22**(6), 6868–6873 (2014).
12. K. X. Li, Y. R. Song, Z. H. Yu, R. Q. Xu, Z. Y. Dou, and J. R. Tian, "L-band femtosecond fibre laser based on Bi_2Se_3 topological insulator," Laser Phys. Lett. **12**(10), 105103 (2015).
13. Y. H. Lin, C. Y. Yang, S. F. Lin, W. H. Tseng, Q. Bao, C. I. Wu, and G. R. Lin, "Soliton compression of the erbium-doped fiber laser weakly started mode-locking by nanoscale p-type Bi_2Te_3 topological insulator particles," Laser Phys. Lett. **11**(5), 055107 (2014).
14. Z. C. Luo, M. Liu, H. Liu, X. W. Zheng, A. P. Luo, C. J. Zhao, H. Zhang, S. C. Wen, and W. C. Xu, "2 GHz passively harmonic mode-locked fiber laser by a microfiber-based topological insulator saturable absorber," Opt. Lett. **38**(24), 5212–5215 (2013).
15. L. Gao, T. Zhu, W. Huang, and Z. Q. Luo, "Stable, ultrafast pulse mode-locked by topological insulator Bi_2Se_3 nanosheets interacting with photonic crystal fiber: from anomalous dispersion to normal dispersion," IEEE Photonics J. **3**(3), 94–99 (2015).
16. B. Guo, Y. Yao, Y. F. Yang, Y. J. Yuan, L. Jin, B. Yan, and J. Y. Zhang, "Dual-wavelength rectangular pulse erbium-doped fiber laser based on topological insulator saturable absorber," Photonics Res. **3**(3), 94–99 (2015).
17. B. Guo, Y. Yao, J. J. Tian, Y. F. Zhao, S. Liu, M. Li, and M. R. Quan, "Observation of bright-dark soliton pair in a fiber laser with topological insulator," IEEE Photonics Technol. Lett. **27**(7), 701–704 (2015).
18. J. Sotor, G. Sobon, W. Macherzynski, and K. M. Abramski, "Harmonically mode-locked Er-doped fiber laser based on a Sb_2Te_3 topological insulator saturable absorber," Laser Phys. Lett. **11**(5), 055102 (2014).
19. H. Y. Xu, X. J. Wan, Q. J. Ruan, R. H. Yang, T. J. Du, N. Chen, Z. P. Cai, and Z. Q. Luo, "Effects of nanomaterial saturable absorption on passively mode-locked fiber lasers in an anomalous dispersion regime: simulations and experiments," IEEE J. Sel. Top. Quantum Electron. **24**(3), 1–9 (2018).
20. Y. H. Xu, H. H. Xie, G. B. Jiang, L. L. Miao, K. Wang, S. Y. Tang, X. F. Yu, H. Zhang, and Q. L. Bao, "Bilayer bismuth selenide nanoplatelets based saturable absorber for ultra-short pulse generation," Opt. Commun. **395**, 55–60 (2017).
21. N. N. Xu, N. Ming, X. L. Han, B. Y. Man, and H. N. Zhang, "Large-energy passively Q-switched Er-doped fiber laser based on CVD-Bi_2Se_3 as saturable absorber," Opt. Mater. Express **9**(2), 373–383 (2019).
22. J. Li, Q. Y. Chen, K. D. Niu, R. Y. Sun, and H. N. Zhang, "Passively mode-locked ytterbium-doped fiber laser based on SnS_2 as saturable absorber," IEEE Photonics J. **9**(6), 1–7 (2017).
23. D. Mao, X. Y. She, B. B. Du, W. D. Zhang, K. Song, X. Q. Cui, B. Q. Jiang, T. Peng, and J. L. Zhao, "Erbium-doped fiber laser passively mode locked with few-layer WSe_2/$MoSe_2$ nanosheets," Sci. Rep. **6**(1), 23583 (2016).
24. H. Xia, H. P. Li, C. Y. Lan, C. Li, X. X. Zhang, S. J. Zhang, and Y. Liu, "Ultrafast erbium-doped fiber laser mode-locked by a CVD-grown molybdenum disulfide (MoS_2) saturable absorber," Opt. Express **22**(14), 17341–17348 (2014).
25. K. D. Niu, Q. Y. Chen, R. Y. Sun, B. Y. Man, and H. N. Zhang, "Passively Q-switched erbium-doped fiber laser based on SnS_2 saturable absorber," Opt. Mater. Express **7**(11), 3934–3943 (2017).
26. D. Mao, X. Q. Cui, X. T. Gan, M. K. Li, W. D. Zhang, H. Lu, and J. L. Zhao, "Passively Q-switched and mode-locked fiber laser based on a ReS_2 saturable absorber," IEEE J. Sel. Top. Quantum Electron. **24**(3), 1–6 (2018).
27. D. Mao, Y. D. Wang, C. J. Ma, L. Han, B. Q. Jiang, X. T. Gan, S. J. Hua, W. D. Zhang, T. Mei, and J. L. Zhao, "WS_2 mode-locked ultrafast fiber laser," Sci. Rep. **5**(1), 7965 (2015).
28. P. G. Yan, A. J. Liu, Y. S. Chen, J. Z. Wang, S. C. Ruan, H. Chen, and J. F. Ding, "Passively mode-locked fiber laser by a cell-type WS_2 nanosheets saturable absorber," Sci. Rep. **5**(1), 12587 (2015).
29. K. D. Niu, R. Y. Sun, Q. Y. Chen, B. Y. Man, and H. N. Zhang, "Passively mode-locked Er-doped fiber laser based on SnS_2 nanosheets as a saturable absorber," Photonics Res. **6**(2), 72–76 (2018).
30. B. Guo, Q. Lyu, Y. Yao, and P. F. Wang, "Direct generation of dip-type sidebands from WS_2 mode-locked fiber laser," Opt. Mater. Express **6**(8), 2475–2486 (2016).
31. Z. C. Luo, M. Liu, Z. N. Guo, X. F. Jiang, A. P. Luo, C. J. Zhao, X. F. Yu, W. C. Xu, and H. Zhang, "Microfiber-based few-layer black phosphorus saturable absorber for ultra-fast fiber laser," Opt. Express **23**(15), 20030–20039 (2015).
32. Y. Chen, G. B. Jiang, S. Q. Chen, Z. N. Guo, X. F. Yu, C. J. Zhao, H. Zhang, Q. L. Bao, S. C. When, D. Y. Tang, and D. Y. Fan, "Mechanically exfoliated black phosphorus as a new saturable absorber for both Q-switching and mode-locking laser operation," Opt. Express **23**(10), 12823–12833 (2015).

Optics EXPRESS

33. J. Ma, S. B. Lu, Z. N. Guo, X. D. Xu, H. Zhang, D. Y. Tang, and D. Y. Fan, "Few-layer black phosphorus based saturable absorber mirror for pulsed solid-state lasers," Opt. Express **23**(17), 22643–22648 (2015).
34. X. X. Jin, G. H. Hu, M. Zhang, Y. W. Hu, T. Albrowowen, R. C. T. Howe, T. Wu, Q. Wu, Z. Zheng, and T. Hasan, "102 fs pulse generation from a long-term stable, inkjet-printed black phosphorus-mode-locked fiber laser," Opt. Express **26**(10), 12506–12513 (2018).
35. N. Ming, S. N. Tao, W. Q. Yang, Q. Y. Chen, R. Y. Sun, C. Wang, and H. N. Zhang, "Mode-locked Er-doped fiber laser based on PbS/CdS core/shell quantum dots as saturable absorber," Opt. Express **26**(7), 9017–9026 (2018).
36. Y. Zhou, Q. Miao, Y. P. Sun, F. Gel'mukhanov, and C. K. Wang, "Solvent effect on dynamical TPA and optical limiting of BDMAS molecular media for nanosecond and femtosecond laser pulses," J. Phys. B: At., Mol. Opt. Phys. **44**(3), 035103 (2011).
37. C. Bai, L. Wang, H. Wan, L. Li, L. Liu, and J. Pan, "Effects of CF4 content on particle densities and reaction pathways in atmospheric-pressure Ar/CF4 pulsed dielectric barrier discharge plasma," J. Phys. D: Appl. Phys. **51**(25), 255201 (2018).
38. Q. X. Guo, H. P. Si, Z. Y. Lu, X. L. Han, B. Y. Man, D. J. Feng, H. N. Zhang, and S. Z. Jiang, "Passively mode-locked dual-wavelength Er-doped fiber laser based on antimony tin oxide as saturable absorber," Laser Phys. **29**(4), 045801 (2019).
39. B. Guo, "2D noncarbon materials-based nonlinear optical devices for ultrafast photonics," Chin. Opt. Lett. **16**(2), 020004 (2018).
40. P. Yan, R. Y. Lin, S. C. Ruan, A. J. Liu, and H. Chen, "2.95 GHz, femtosecond passive harmonic mode-locked fiber laser based on evanescent field interaction with topological insulator film," Opt. Express **23**(1), 154–164 (2015).
41. N. N. Xu, H. N. Zhang, and B. Y. Man, "Various large-energy soliton operations within an Er-doped fiber laser with bismuth selenide as a saturable absorber," Appl. Opt. **57**(30), 8811–8818 (2018).
42. H. Zhang, C. X. Liu, X. L. Qi, X. Dai, F. Fang, and S. C. Zhang, "Topological insulators in Bi_2Se_3, Bi_2Te_3 and Sb_2Te_3 with a single Dirac cone on the surface," Nat. Phys. **5**(6), 438–442 (2009).
43. B. Guo, Y. Yao, Y. F. Yang, Y. J. Yuan, R. L. Wang, S. G. Wang, Z. H. Ren, and B. Yan, "Topological insulator: Bi_2Se_3/polyvinyl alcohol film-assisted multi-wavelength ultrafast erbium-doped fiber laser," J. Appl. Phys. **117**(6), 063108 (2015).
44. D. Mao, B. Jiang, X. Gan, C. Ma, Y. Chen, C. Zhao, H. Zhang, J. Zheng, and J. Zhao, "Soliton fiber laser mode locked with two types of film-based Bi_2Te_3 saturable absorbers," Photonics Res. **3**(2), A43–A46 (2015).
45. J. Lee, J. Koo, Y. M. Jhon, and J. H. Lee, "A femtosecond pulse erbium fiber laser incorporating a saturable absorber based on bulk-structured Bi_2Te_3 topological insulator," Opt. Express **22**(5), 6165–6173 (2014).
46. Y. Chen, M. Wu, P. Tang, S. Chen, J. Du, G. Jiang, Y. Li, C. Zhao, H. Zhang, and S. Wen, "The formation of various multi-soliton patterns and noise-like pulse in a fiber laser passively mode-locked by a topological insulator based saturable absorber," Laser Phys. Lett. **11**(5), 055101 (2014).
47. Q. Wang, Y. Chen, L. Miao, G. Jiang, S. Chen, J. Liu, X. Fu, C. Zhao, and H. Zhang, "Wide spectral and wavelength-tunable dissipative soliton fiber laser with topological insulator nano-sheets self-assembly films sandwiched by PMMA polymer," Opt. Express **23**(6), 7681–7693 (2015).
48. J. Sotor, G. Sobon, and K. M. Abramski, "Sub-130 fs mode-locked Er-doped fiber laser based on topological insulator," Opt. Express **22**(11), 13244–13249 (2014).
49. J. Bogusławski, G. Soboń, R. Zybała, K. Mars, A. Mikuła, K. M. Abramski, and J. Sotor, "Investigation on pulse shaping in fiber laser hybrid mode-locked by Sb_2Te_3 saturable absorber," Opt. Express **23**(22), 29014–29023 (2015).
50. J. Sotor, G. Sobon, K. Grodecki, and K. M. Abramski, "Mode-locked erbium-doped fiber laser based on evanescent field interaction with Sb_2Te_3 topological insulator," Appl. Phys. Lett. **104**(25), 251112 (2014).
51. J. Boguslawski, J. Sotor, G. Sobon, J. Tarka, J. Jagiello, W. Macherzynski, L. Lipinska, and K. M. Abramski, "Mode-locked Er-doped fiber laser based on liquid phase exfoliated Sb_2Te_3 topological insulator," Laser Phys. **24**(10), 105111 (2014).
52. J. Sotor, G. Sobon, W. Macherzynski, P. Paletko, K. Grodecki, and K. M. Abramski, "Mode-locking in Er-doped fiber laser based on mechanically exfoliated Sb_2Te_3 saturable absorber," Opt. Mater. Express **4**(1), 1–6 (2014).
53. J. Boguslawski, G. Sobon, R. Zybala, and J. Sotor, "Dissipative soliton generation in Er-doped fiber laser mode-locked by Sb_2Te_3 topological insulator," Opt. Lett. **40**(12), 2786–2789 (2015).
54. W. Liu, L. Pang, H. Han, W. Tian, H. Chen, M. Lei, P. Yan, and Z. Wei, "Generation of dark solitons in erbium-doped fiber lasers based Sb_2Te_3 saturable absorbers," Opt. Express **23**(20), 26023–26031 (2015).